

CIRRUS SPECTRA OF LOW SURFACE BRIGHTNESS REGIONS

M. Juvela¹, K. Mattila¹, D. Lemke²

¹Helsinki University Observatory, P.O. Box 14, SF-00014 University of Helsinki, Finland

²Max-Planck-Institut für Astronomie, Königstuhl 17, D-69117 Heidelberg, Germany

ABSTRACT

We have studied the galactic cirrus in low surface brightness regions using ISOPHOT raster maps at $90\ \mu\text{m}$, $150\ \mu\text{m}$ and $180\ \mu\text{m}$. Observations are used to determine dust emission spectra and dust temperatures. The data extend to longer wavelengths than IRAS observation. Compared with DIRBE data the resolution and the sensitivity are better and this makes it possible to study faint cirrus emission in individual fields.

We will discuss the calibration of the observations and present results of a comparison between ISOPHOT and DIRBE surface brightness values. The correspondence was found to be better than $\sim 30\%$. At $90\ \mu\text{m}$ the ISOPHOT surface brightnesses tend to be slightly higher than the DIRBE values while at longer wavelength the situation is reversed.

Surface brightness variations caused by cirrus fluctuations make it possible to determine the spectrum of the dust emission. Cirrus spectra were obtained for six fields with surface brightnesses in the range $1\text{--}2\ \text{MJy sr}^{-1}$ after the Zodiacal light and the contribution of extragalactic sources have been subtracted.

Assuming ν^2 emissivity law the dust temperatures are in the range $18\text{--}20\ \text{K}$. Temperature variations can be seen even within individual fields. These values are higher than values from DIRBE but this can be explained by differences in the calibration.

Key words: ISO; infrared astronomy; cirrus.

1. INTRODUCTION

At wavelengths longer than $\sim 100\ \mu\text{m}$ the far-infrared emission of the Galaxy is dominated by thermal emission from large dust particles that are in thermal equilibrium with the interstellar radiation field. Dust temperatures determined from DIRBE measurements are typically $16\text{--}19\ \text{K}$ (e.g. Lagache et al. 1998; Dwek et al. 1997) in rough agreement with model predictions (e.g. Draine & Anderson 1985).

Most previous FIR dust temperature determinations have been based on COBE observations. These have,

however, poor spatial resolution and in low surface brightness regions the sensitivity of the detectors becomes a limiting factor so that only an average dust spectrum over a large area can be determined.

We use ISOPHOT observations to study the spectrum of galactic cirrus in regions selected for their low surface brightness. Because of the better sensitivity and angular resolution of the ISOPHOT instrument it is possible to determine the cirrus spectrum in these fields based on the cirrus intensity variations. In this way constant or slowly varying components, e.g. Zodiacal light, can be eliminated.

The determination of the cirrus spectrum is important also for extragalactic studies where the galactic foreground emission must be separated. In future work the same fields will be used to estimate the FIR component of the cosmic background radiation.

We start by presenting the observations used in this study. After that calibration differences between ISOPHOT and DIRBE observations are discussed. Calibration issues are obviously essential for the determination of the spectra and the dust temperatures. Finally, the method used to derive the cirrus spectra and the derived dust temperatures are presented. A ν^2 dust emissivity law will be assumed throughout this paper.

2. OBSERVATIONS

The cirrus spectra were determined in six fields that had been observed at $90\ \mu\text{m}$, $150\ \mu\text{m}$ and $180\ \mu\text{m}$ with the ISOPHOT instrument (Lemke et al. 1996) aboard the ISO satellite (Kessler et al. 1996). The observation consist of PHT22 raster maps. Detailed description of the observations is given in Table 1. Data reduction was done using the ISOPHOT Interactive Analysis software package (PIA) (Gabriel et al. 1997) version 8.0. In the following the analysis is based on measurements reduced to the AAP level.

Flatfielding was done outside PIA using custom routines that also removed slow drifts of the detector pixels relative to each other. Good flat fielding is not critical for the determination of the spectra but it will reduce the noise in the subsequent steps.

Table 1. Description of the ISOPHOT maps used to determine the cirrus spectra. The columns are: (1) name of the field, (2)-(3) coordinates of the centre of each field, (4)-(5) galactic coordinates, (6) map area, (7) ISOPHOT filter, (8) number of raster positions, (9) step between adjacent raster positions and (10) integration time. The distance of adjacent scans was the same as the raster step used along the scan line.

Field (1)	Map Centre		l (4)	b (5)	Area (square degrees) (6)	Filter (7)	Rasters (8)	Step (arcsec) (9)	t_{int} (s) (10)
	RA(2000.0) (2)	DEC(2000.0) (3)							
VCN	15 15 21.7	+56 28 58	91.76	51.42	0.030	C_90	10×4	90	46
						C_135	10×4	90	46
						C_180	10×4	90	46
VCS	15 15 53.1	+56 19 30	91.27	51.40	0.023	C_90	21×2	90	46
						C_135	21×2	90	46
						C_180	21×2	90	46
NGPN	13 43 53.0	+40 11 35	86.82	73.61	0.27	C_90	32×4	180	23
						C_135	32×4	180	27
						C_180	32×4	180	27
NGPS	13 42 32.0	+40 29 06	87.88	73.26	0.53	C_180	15×15	180	32
	13 49 43.7	+39 07 30	81.49	73.30	0.27	C_90	32×4	180	23
						C_135	32×4	180	27
EBL22	02 26 34.5	-25 53 43	215.78	-69.19	0.19	C_90	32×3	180	23
						C_135	32×3	180	27
						C_180	32×3	180	27
EBL26	01 18 14.5	01 56 40	135.89	-60.66	0.27	C_90	32×4	180	23
						C_135	32×4	180	23
						C_180	32×4	180	23

3. COMPARISON WITH DIRBE SURFACE BRIGHTNESS VALUES

The results presented in this paper are based on the calibration performed with Fine Calibration Source (FCS) measurements. The absolute calibration of ISOPHOT observations has been estimated to be better than 30% (Klaas et al. 1998). Klaas & Richards (1999) recently reported for both C100 and C200 accuracies better than 20% relative to DIRBE. These results apply to fields with surface brightness above $\sim 5 \text{ MJy sr}^{-1}$ while several of our C200 maps are below 4 MJy sr^{-1} . It is therefore useful to compare our observations with DIRBE data especially as the calibration accuracy is essential for the determination of the cirrus spectra.

The DIRBE and ISOPHOT calibration was studied in the case of the fields NGPS, NGPN, EBL22, and EBL26 (see Table 1). Three methods were used to perform the comparison:

1. *Comparison of absolute surface brightness levels.* The ISOPHOT maps were compared with DIRBE ZSMA (*Zodi-Subtracted Mission Average*) data to which Zodiacal light was added according to the model given by Leinert et al. (1998). Using the DIRBE weekly maps observed with the same solar elongation as the ISO data did not change the results significantly. Because of the lower noise we chose to use the ZSMA data. Both DIRBE ZSMA and ISO were colour corrected assuming a $\nu^2 B_\nu$ spectrum with $T_{\text{dust}}=18 \text{ K}$. The zodiacal light estimates were colour corrected assuming black body spectrum with $T_{\text{dust}}=270 \text{ K}$ (Abraham et al. 1998; Abraham et al. 1999). Corresponding curves fitted to the DIRBE ZSMA $100 \mu\text{m}$, $140 \mu\text{m}$ and $240 \mu\text{m}$

data and the zodiacal light estimates were used to derive the DIRBE surface brightness estimates interpolated to the wavelength of the ISO observations. The average ISO flux density was compared with the derived DIRBE values calculated as the average over ISO map and weighted by the DIRBE beam. The result is the surface brightness ratio $S(\text{DIRBE})/S(\text{ISOPHOT})$.

2. *Direct comparison of the surface brightness variations* in ISOPHOT and DIRBE ZSMA maps. All data were first colour corrected for a spectrum $\nu^2 B(\nu)$ with $T_{\text{dust}}=18.0 \text{ K}$. For each DIRBE pixel the data were interpolated to the wavelength of the ISOPHOT observations and the corresponding ISOPHOT surface brightness estimate was calculated as a weighted average over the DIRBE beam. Linear fit was done to these points to derive the slope between the surface brightness values $k = \Delta S(\text{DIRBE})/\Delta S(\text{ISOPHOT})$.
3. *Comparison via IRAS.* Linear relations were established between the IRAS $100 \mu\text{m}$ data and the ISO observations and between the IRAS data and the DIRBE ZSMA data interpolated to the wavelength of the ISO observations using a fitted curve $\nu^2 B_\nu(T=18 \text{ K})$. For each IRAS ISSA map pixel inside the field the corresponding ISO surface brightness was calculated as an average weighted with a Gaussian with FWHM $\sim 5 \text{ arcmin}$. The relation between IRAS and DIRBE surface brightnesses was determined with a similar method but over an area with radius ~ 2 degrees where for each DIRBE pixel the average IRAS value was calculated by weighting with the DIRBE beam. The slopes of these two linear relations $\Delta S(\text{DIRBE})/\Delta S(\text{IRAS}(100 \mu\text{m}))$ and $\Delta S(\text{IRAS}(100 \mu\text{m}))/\Delta S(\text{ISOPHOT})$ give the ratio between DIRBE and ISO scales, $k =$

$$\Delta S(\text{DIRBE})/\Delta S(\text{ISOPHOT}).$$

Method (1) suffers from the small size of the ISOPHOT maps which means that for each DIRBE pixel a large portion of the flux comes from outside the area mapped with ISOPHOT.

Method (2) is even more affected by the limited map sizes and the large size of the DIRBE beam since we must determine the relation between brightness variations. However, NGPN and NGPS form together a 3.1 degrees long strip where the surface brightness gradient is along the longer side of the map. Here the fact that the ISO map is narrow compared with the DIRBE beam should not lead to significant errors. On the other hand, in EBL26 the surface brightness drops quickly outside the bright region in the northern part of the map. The surface brightness variation is not resolved by DIRBE beam and the values $\Delta(\text{DIRBE})/\Delta(\text{ISOPHOT})$ obtained would be underestimated. In EBL22 and NGPN the method does not work because of the lack of sufficient surface brightness variations.

Methods (2) and (3) are not affected by the presence of zodiacal light. The last method uses IRAS ISSA maps as an intermediate step and is therefore much less affected by the poor resolution of the DIRBE data. It allows also the use of DIRBE data over a much larger area and thereby reduces the effect of the large noise present in 140 μm and 240 μm DIRBE observations. In these low surface brightness regions the error estimates of 140 μm and 240 μm DIRBE measurements exceed 50%. On the other hand, the method is based on the assumption that the ratio of the emission at 100 μm and at other wavelengths remains constant.

The results are given in Table 2. It can be seen that DIRBE and ISOPHOT surface brightness values agree typically to within 30%. However, at 90 μm the ISOPHOT surface brightness tends to be above the value predicted from DIRBE observations while at longer wavelengths the situation is reversed. The extrapolation of the DIRBE values to 90 μm using the modified black body fitted to three longer wavelengths may not be entirely justified and may lead to underestimation of the surface brightness. Also, in these faintest regions the accuracy of the DIRBE 140 μm and 240 μm is poor and a reliable comparison with ISOPHOT C200 values is difficult. The modified black body curves fitted to DIRBE data are determined mostly by the 100 μm DIRBE value which has significantly smaller error estimates than the two longer wavelengths, and the assumed dust temperature, $T=18.0\text{K}$. Increasing the temperature by one degree would increase k at 90 μm by some 5% and decrease it at longer wavelengths by some 15%.

In spite of uncertainties the results suggest that the dust temperatures derived from ISOPHOT observations are, because of calibration differences, higher than those based on DIRBE data. Using PIA versions prior to 8.0 the differences between ISOPHOT and DIRBE surface brightnesses were typically larger by some 20%.

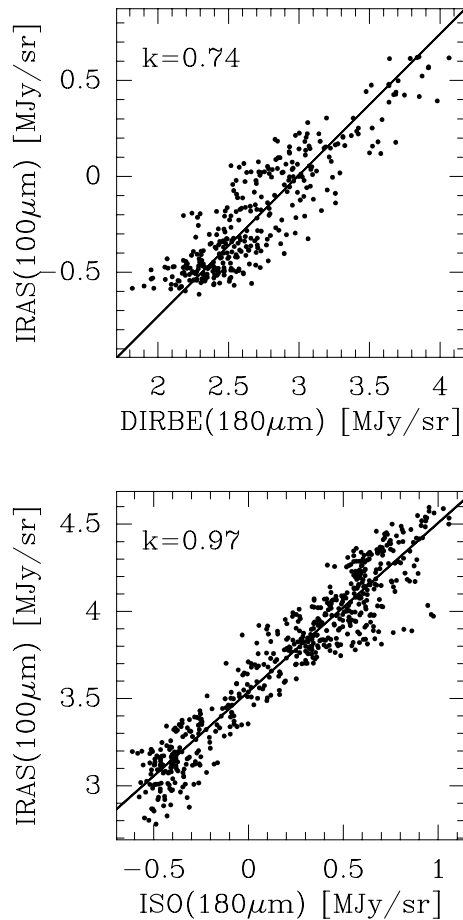


Figure 1. Determination of the relative scales of the ISOPHOT and DIRBE maps using IRAS 100 μm ISSA maps as an intermediate step. The ISOPHOT map is the 180 μm map of the field NGPS. The upper frame shows linear fit between IRAS 100 μm surface brightness values and the DIRBE values interpolated to 180 μm . The lower frame shows the corresponding fit between IRAS 100 μm and ISOPHOT maps. The slopes of the fitted lines (shown in figures) can be combined to get the value shown in column 5 of Table 2.

4. CIRRUS SPECTRA

As the first step all data were colour corrected in order to derive monochromatic surface brightness values at the reference wavelengths of the filters. Correction was done for spectrum $\nu^2 B_\nu(T = 18\text{K})$ which approximates the expected cirrus spectrum. A large fraction of the observed surface brightness values is due to Zodiacal light. Since we will study only the relative surface brightness variations the Zodiacal light is eliminated from the analysis and it does not affect the required colour correction.

In the calculations the 180 μm maps are used as the reference. For each 180 μm pixel the corresponding surface brightness value at another wavelength is calculated as a weighted average. The spatial weighting is done with a Gaussian with FWHM ≈ 100 arcsec and the individual measurements are also weighted

Table 2. The ratios k between the DIRBE and ISO flux density scales. The columns are: (1) the name of the field, (2) wavelength of ISO observations, (3) mean surface brightness of the ISO map, (4) k from the comparison of absolute surface brightnesses, (5) k obtained from direct comparison of surface brightness variations and (6) k obtained via 100 μm ISSA maps. Formal errors from the least squares fits are shown in parentheses. For the first method (i.e. column 4) the numbers given in parentheses give the dispersion in the DIRBE surface brightness values interpolated to the wavelength of the ISO observations

Map	λ (μm)	$\langle S \rangle$ (MJy/sr)	$S(\text{DIRBE})/S(\text{ISOPHOT})$	$\Delta S(\text{DIRBE})/\Delta S(\text{ISO})$	via IRAS
(1)	(2)	(3)	(4)	(5)	(6)
EBL22	90	5.6	0.81(0.01)		
	150	3.4	1.28(0.03)		
	180	2.7	1.42(0.05)		
EBL26	90	14.3	0.84(0.02)		0.88(0.10)
	150	9.1	1.04(0.05)		1.09(0.12)
	180	7.4	1.09(0.03)		1.27(0.14)
NGPS	90	5.7	0.69(0.06)	0.69(0.10)	0.70(0.05)
	150	3.7	0.94(0.15)	1.68(0.15)	1.43(0.11)
	180	3.1	1.04(0.02)	1.59(0.15)	1.40(0.10)
NGPN	90	5.0	0.67(0.02)		
	150	3.6	0.97(0.04)		
	180	2.7	1.19(0.11)		
	180 ¹	2.6	1.21(0.07)		
NGPN & NGPS	90	5.2	0.67(0.02)	0.63(0.21)	0.75(0.06)
	150	4.1	0.92(0.04)	0.91(0.34)	1.56(0.13)
	180	3.3	1.08(0.12)	0.84(0.33)	1.53(0.11)

¹ the larger 180 μm map

according to their error estimates. The calculated values are plotted against the 180 μm surface brightness and a straight line is fitted to the points with a least squares algorithm that takes into account the error estimates on both axes. The procedure is repeated for all maps and the slopes of the fitted lines provide the emission spectrum i.e. for each observed wavelength the relative intensity with respect to the 180 μm emission.

Figure 2 shows as an example the relations between 180 μm and 90 μm and 180 μm and 150 μm surface brightness values in the field EBL26. The fitted least square lines are also shown. Zodiacal light will appear merely as an offset and does not affect the slopes that determine the cirrus spectrum. Furthermore, zodiacal light is weak at 180 μm and we are looking only for variations correlated with 180 μm emission.

Galactic cirrus is the dominant source of brightness fluctuations and therefore the spectra obtained characterize the galactic cirrus emission. However, in low surface brightness regions there may be a significant contribution from faint extragalactic sources. The DIRBE (Hauser et al. 1998) and FIRAS (Fixen et al. 1998) experiments indicated a FIR cosmic infrared background flux of 1 MJy sr⁻¹ between 100 and 240 μm . In fields like EBL22 this would mean that at 180 μm about one third of the surface brightness is due to extragalactic sources. Since the cirrus spectra are determined from the brightness variations we must consider the brightness fluctuations caused by these sources in relation to the cirrus fluctuations.

The cirrus power spectrum is proportional to B_0/k^3 , where B_0 is the cirrus brightness and k the spatial frequency (Gautier et al. 1992). In other words, cirrus fluctuations decrease rapidly as we move to fainter cirrus regions and smaller spatial scales. Lagache &

Puget (1999) have reported a detection of the extragalactic background fluctuations at 175 μm in the Marano 1 field that has cirrus surface brightness comparable to our fields. Even after removal of detected sources they found at scales below 10 arcmin fluctuations in excess of the expected cirrus contribution. This was interpreted to be caused by point sources below the detection limit.

The larger dimension of our maps is typically 1.5 degrees and most of the surface brightness variations can be expected to be due to cirrus. This is particularly clear in fields NGPS and EBL26 where there is a clear intensity gradient along the mapped strip consistent with the larger scale cirrus distribution visible in IRAS maps. On the other hand, the field EBL22 is remarkably flat and it is conceivable that in the absence of large cirrus structures the extragalactic point sources could affect the derived spectrum. The small dynamic range means, however, that in this case the accuracy of the derived spectrum is not very good. The fields VCN and VCS were observed close the bright galaxy NGC 5907 and the VCS field actually extends over the centre of the galaxy. Pixels that were clearly affected by the emission from NGC 5907 were first discarded but it is still possible that the derived spectra are affected by emission of the galaxy. Because of the small field size (~ 10 arcmin) the VCN spectrum could be affected by faint extragalactic sources.

The spectra obtained for the six fields are presented in Figure 3. The error bars include the error estimates obtained from the fitting procedure and a further 10% error representing the error in the relative calibration of the observations made with different filters. Modified Planck curves, $\nu^2 B_\nu(T)$, were fitted to the data and the dust temperatures obtained are shown in the figure.

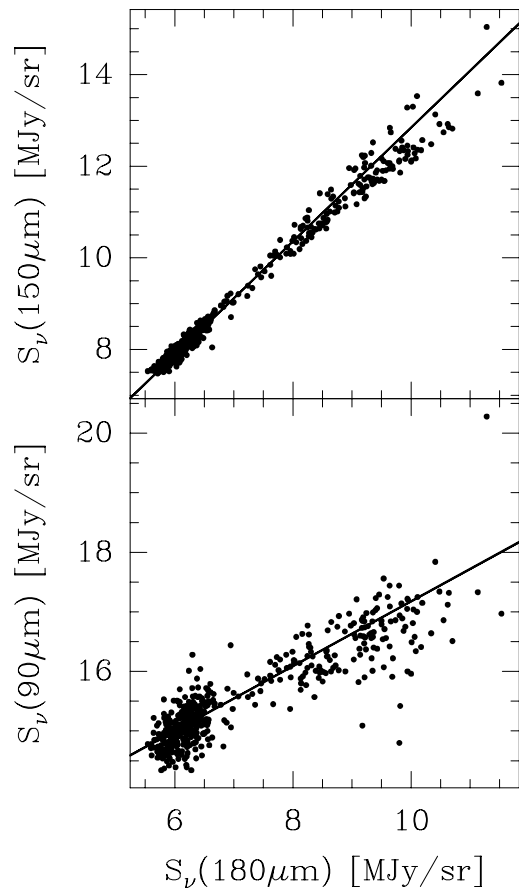


Figure 2. Plots of the $90\ \mu\text{m}$ and the $150\ \mu\text{m}$ surface brightness values in the EBL26 field as function of $180\ \mu\text{m}$ surface brightness. The fitted least squares lines are also shown. The slopes of these lines give the ratio between surface brightnesses at different wavelengths i.e. the spectrum of the cirrus emission.

5. DISCUSSION

We have determined cirrus dust temperatures in six fields with low surface brightness. The derived dust temperatures, $\sim 18\text{--}20\ \text{K}$, are higher than the typical temperatures estimated for galactic dust from DIRBE and FIRAS experiments assuming the same ν^2 emissivity law. However, the values are still within the range found in these studies. Lagache et al. (1998) found an average temperature of $17.5\ \text{K}$ while higher temperatures were mostly associated with star forming regions. Temperatures exceeding $20\ \text{K}$ were seen only towards the galactic centre and some prominent star forming regions although the scatter in the temperatures is more than $1\ \text{K}$ at all galactic latitudes.

Our fields are all at high galactic latitudes (see Table 1). Based on COBE measurements at $100\text{--}240\ \mu\text{m}$ Boulanger et al. (1996) derived average dust temperatures of $T = 17.5\ \text{K}$ for regions at $|b| > 30$ degrees. Earlier FIRAS estimates (Reach et al. 1995) also suggested similar or lower values. However, based on the DIRBE $140\ \mu\text{m}$ to $240\ \mu\text{m}$ ratios Dwek et al. (1997) reported colour temperatures of $T \sim 19\ \text{K}$ for regions

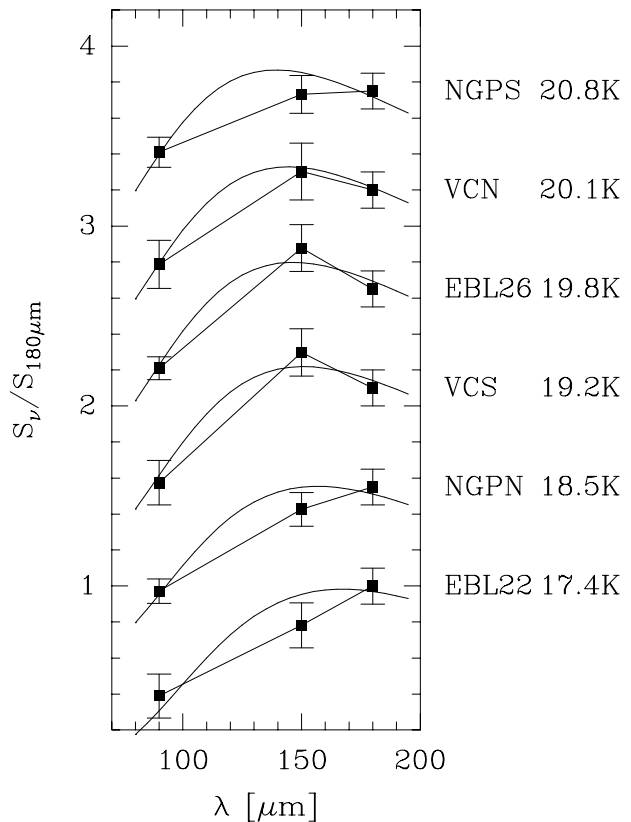


Figure 3. Cirrus spectra derived from the six observed fields. The error estimates contain the statistical errors provided by the fitting procedure and a further 10% error representing the uncertainty of the relative calibration between the filters. The solid lines show the fitted modified black body curves, $\nu^2 B_\nu(T)$.

with $|b| > 45$ degrees.

In Section 3. we found systematic differences between ISOPHOT and DIRBE calibrations. Compared with DIRBE the ISOPHOT surface brightnesses were found to be higher at $90\ \mu\text{m}$ and lower at longer wavelengths. According to Table 2 adopting the DIRBE calibration would increase our $90\ \mu\text{m}$ data by up to 30% relative to the longer wavelengths. This would reduce the estimated dust temperature by $\sim 1.5\ \text{K}$. Therefore the temperature difference between DIRBE and our results can be explained entirely by the difference in calibration.

Our temperature determinations are based on data at three wavelengths: $90\ \mu\text{m}$, $150\ \mu\text{m}$ and $240\ \mu\text{m}$. The emission at wavelengths $\lambda > 100\ \mu\text{m}$ can be explained by classical grains in equilibrium with the interstellar radiation field. Smaller grains that are transiently heated to higher temperatures are responsible for the emission at shorter wavelengths. Based on both observations and theoretical calculations the contribution from transiently heated particles is significant already at $60\ \mu\text{m}$ and may extend even to slightly longer wavelengths (Sodroski et al. 1994; Dwek et al. 1997; Desert et al. 1990). The ISOPHOT $90\ \mu\text{m}$ filter is wide enough to pick up some radiation from wavelengths down to $\sim 60\ \mu\text{m}$ and our observations may be affected to a small degree by this other grain popula-

tion. Our temperature estimates do not correspond exactly to the equilibrium temperature of large dust particles but the bias towards higher temperatures is expected to be small.

In the low surface brightness regions the accuracy of DIRBE measurements is not very good and one can obtain only the average spectrum of a very large area. Because of the better resolution and sensitivity of ISOPHOT we have been able to study the cirrus spectrum in separate, small regions. Adopting the ISOPHOT calibration the accuracy of the temperature estimates is ~ 1 K. For example, the 2 K difference between the adjacent fields NGPS and NGPN is likely to be true.

ACKNOWLEDGMENTS

The work was supported by the Academy of Finland Grant no. 1011055 and funding from DLR and MPG in Germany.

REFERENCES

- Ábraham P., Leinert C.H., Lemke D., 1998, Astron. Gesellschaft Meeting Abstracts 14, E08
- Ábraham P., Leinert C., Acosta-Pulido J. et al. 1999, ESA SP-427, Vol. 1, 145
- Boulanger F., Abergel A., Bernard J.P. et al. 1996, A&A 312, 256
- Dwek E., Arendt R.G., Fixsen D.J. et al. 1997, ApJ 475, 565
- Draine B.T., Anderson N. 1985, ApJ 292, 494
- Desert F.-X., Boulanger F., Puget J.-L. 1990, 237, 215
- Fixsen, D.J., Dwek, E., Mather, J.C. et al. 1998, ApJ 508, 123
- Gabriel C., Acosta-Pulido J., Heinrichsen I. et al., in Hunt G., Payne H.G. (eds), ADASS VI, ASP conference series, vol. 125,
- Gautier, C., III, Boulanger, F., Perault, M., Puget, J.L. 1992, AJ 103, 1313
- Hauser M.G., Arendt R.G., Kelsall T. et al. 1998, ApJ 508, 25
- Kessler M.F., Steinz J.A., Anderegg M.E. et al. 1996, A&A 315, L27
- Klaas U., Laureijs, R.J., Radovich, M., Schulz, B. 1998, 'ISOPHOT Calibration Accuracies', http://www.iso.vilspa.esa.es/users/expllib/PHT_top.html
- Klaas U., Richards P. 1999, 'Release Note for ISOPHOT OLP version 8.4', http://www.iso.vilspa.esa.es/users/expllib/PHT_top.html
- Lagache G., Abergel A., Boulanger F., Puget J.-L. 1998, A&A 333, 709
- Lagache G., Puget J.L. 1999, A&A (submitted), astrp-ph/9910255
- Leinert, C.H., Bowyer, S., Haikala, L. K., et al. 1998, A&AS 127, 1
- Lemke D., Klaas U., Abolins J., et al. 1996, A&A 315, L64
- Reach W.T., Dwek E., Dixsen D.J. et al. 1995, ApJ 451, 188
- Sodroski T.J., Bennett C., Boggess N., et al. 1994, ApJ 428, 638